Shape resonances in photoemission for CO molecules adsorbed on metallic surfaces: A model including backscattering

P. Budau* and G. Raşeev†
Laboratoire de Photophysique Moléculaire du Centre National de la Recherche Scientifique, Laboratoire associé à l'Université de Paris–Sud, Bâtiment 213, 91405 Orsay, France
(Received 14 November 1994; revised manuscript received 23 February 1995)

The photoionization differential cross section and the circular dichroism in the angular distribution (CDAD) have been calculated for the case of a theoretical model of on-top chemisorption of CO molecules on Ni(111) and Ni(100) surfaces. The results show a stability with respect to the atomic basis set used provided one includes the polarization functions and are sensitive to orthogonalization to the first σ or π valence virtual orbitals having, respectively, predominant 4*s* character of the Ni atom or $2\pi^*$ character of the CO molecule. The backscattering of photoelectrons modifies the results only slightly. This theoretical model gives, for valence shell ionization of adsorbed CO on metals, 4σ and 5σ excitation cross section and $4\sigma/5\sigma$ branching ratio in agreement with experiment. For *s* polarization of light the σ transitions to the well known $\varepsilon\sigma$ resonance are forbidden and we show that an unknown $\varepsilon\pi$ shape resonance, corresponding in particular to the $5\sigma\rightarrow\varepsilon\pi$ transition, can explain the experimental spectrum. This interpretation is in contradiction with the usual picture based on $\sigma\rightarrow\varepsilon\sigma$ resonant and $1\pi\rightarrow\varepsilon\pi$ nonresonant transitions, corresponding to orthogonal electron emission directions. The selection rules for the transition of oriented-in-space molecules should explicitly incorporate the presence of two degenerate $\varepsilon\sigma$ and $\varepsilon\pi$ continua. We also show that the normalization procedure used in the measurements of CDAD can sometimes give spurious results.

I. INTRODUCTION

The study of the photoionization of adsorbates either using photoelectron spectra (PES) or photoionization spectra (PIS) was, since the beginning, based on a theoretical model of oriented-in-space molecules[1–6] derived from gas-phase calculations. For physisorbed species, the molecule-surface interaction is of van der Waals type and the electronic cloud of the adsorbate is not significantly perturbed. The oriented-in-space model would be ideal if the adsorbate nuclear motion would not play an essential role. In a reasonable theoretical model for physisorbed species, one has to introduce simultaneously the electronic and nuclear motions particularly hindered rotation.[7] For chemisorbed species, one should take into account the electronic adsorbate-surface interaction and the nuclear motion seems to be less important. The currently used models restrict the electronic interaction to one metallic atom in interaction with the adsorbate.[5] Recently we have used, for an oriented-in-space model, a step potential function to model the backscattering of the photoelectrons by the surface after photoionization (Budau, Büchner, and Raseev,[8] hereafter referred to as BBR). The model implies two stages in the calculation. First, we obtain the photoionization transition moment for an oriented-in-space molecule or a cluster including atoms from the surface. We then modify this moment by performing interference between contributions from direct electrons and those backscattered on a step potential representing the surface. In BBR, the calculations were done for CO without including the chemical interaction with the metal. They showed a very strong influence of the backscattering but were in disagreement with the experimental data. The step potential was adapted from standard quantum mechanics[9,10] and is justified for low-kinetic-energy electrons. The two-stages approach is standard when introducing the backscattering, and was used for example in the single-scattering formalism (see, e.g., Ref. 11). To introduce the backscattering of electrons, one can also use a smooth step function that will eventually avoid spurious resonances. (See, e.g., Jennings, Jones, and Weinert[12] and Leung and George.[13])

In the last 25 years many experiments have been performed for the photoionization of CO molecule adsorbed on a variety of metals (Ni, Cu, Co, Pt, Pd, etc.[14–18]). When interpreting the experimental spectrum, one usually compares the PES/PIS in the gas phase with the corresponding spectrum of adsorbed molecules. This comparison would be meaningful if the change originating from the surface mainly had a single or a predominant origin. First, among the changes at adsorption, one should consider the orientation in space of the adsorbed molecule and the modification of the strength of the electronic transition moment usually introduced in the framework of a local axial symmetry model (e.g., linear cluster of molecule-surface atom). To take into account the orientation in a qualitative way, the simplest approach is the use of selection rules for dipole transitions of oriented-in-space molecules discussed in detail by Plummer and Eberhardt.[14] For example, an ionization from a σ orbital accesses two energy degenerate electronic continua, namely $\varepsilon\sigma$ and $\varepsilon\pi$. Depending on the particular strength of the transition moment, one or both continua will contribute to the differential cross section. Usually one considers only $\sigma\rightarrow\varepsilon\sigma$ resonant and $1\pi\rightarrow\varepsilon\pi$ nonresonant transitions and neglects the $\sigma\rightarrow\varepsilon\pi$, $\pi\rightarrow\varepsilon\sigma$, and $\pi\rightarrow\varepsilon\delta$

ones. In this paper, we show that for *s*-polarized light this is a crude approximation. Second, the selection rules[14] can be used only for molecules lying or standing on surface when the axial symmetry of the overall system is conserved. The introduction of full local symmetry of the adsorption site, that for on-top diatomic adsorbates can be nonaxial, modifies these rules. (See, e.g., Kuznetsov, Raseev, and Cherepkov;[19] see also the gas-phase study of nonlinear molecules by Chandra.[20]) Finally, the nuclear motion of an adsorbed molecule like, for example, libration (called also hindered rotation) can change the direction of the molecular axis and significantly modify the spectra particularly for the physisorbed species.[7]

A more elaborate procedure of interpretation of experimental data consists in the incorporation of results of theoretical models, like the oriented-in-space one, in the experimental analysis, for example, to normalize the data or to obtain the value of the light polarization. The use of the theoretical information in the interpretation of the experimental data is sometimes ambiguous. An example is the orientation of adsorbed CO molecular axis about the surface normal. To obtain this information one usually replaces the surface normal with the incident direction of light and assimilates the angle between the molecular axis and the photon direction to that between the molecular axis and the surface normal. In fact, an accurate model should introduce three directions (photon, surface, and molecule) as it was done by Büchner and Raseev.[7]

In this paper, we combine the one metallic atom-adsorbed molecule linear-cluster model, similar to Dubs, Smith, and McKoy,[5] with the backscattering model based on a structureless step potential that we have recently adapted (BBR) from the *e*-molecules collisions.[9,10] The approximation of a linear cluster is justified, at least to the first order for on-top sites, because it is the local perturbation generated by the nearest metallic atom that changes the interactions in the adsorbed molecule and modifies the ionization potential and the escaping direction of the photoelectron. The simple approximation of the structureless surface in backscattering is justified for low-kinetic-energy electrons that have their associate wave spreading among many surface atoms. Consequently the electron feels an average structureless potential as our step function. The present model was designed for molecules adsorbed normal to the surface on on-top sites, like CO on Ni, having the highest-order local-symmetry axis in this direction. The surfaces considered in this paper are Ni(100) and Ni(111) having fourfold and sixfold local-symmetry axes. The normal position of the CO molecule is supported by the experimental analysis, which considers an upright position of CO molecule with an uncertainty of the order of 15°.[21,22] The above picture is valid provided the influence of electrons from the band structure of the metal is not significant. Also, one neglects here the nuclear motion of the adsorbate, of the surface and bulk atoms. For the adsorbate itself, there are several such motions: the internal vibration that will not change the present picture giving rise only to some smoothening of observables, the libration and precession (called also hindered rotation) of the adsorbate that will influence the ejection direction of the electron, and the translation of the adsorbate parallel to the surface. The libration and precession have been taken into account in a recent model[7] but, as the emphasis in this paper is on electronic interaction and backscattering, they will be neglected in the following. Other nuclear degrees of freedom like molecule-surface and internal vibrations can be introduced but were not considered here. The influence of surface and volume phonons can be thought as introducing some nonspecific average over the results and was not introduced either.

In the framework of the described model, we have calculated the differential photoionization cross sections for 5σ, 1π, and 4σ excitations, $5\sigma/4\sigma$ branching ratio, and circular dichroism in the angular distribution[3,4,23–25] (CDAD is the difference between right and left light polarized differential cross sections.) The calculations were done in the region of shape resonances for two experimental set ups corresponding to *p* and *s* polarization light. The relative contributions of the chemical bond and backscattering of the electrons to these observables and the changes in the CDAD spectrum due to its normalization to the total intensity will be discussed.

Through this paper, we will use in our discussions, but not in the calculations, the gas-phase ordering of the CO molecule orbitals namely 5σ, 1π, and 4σ corresponding to the final ionic states of CO $X^2\Sigma^+$, $A^2\Pi$, and $B^2\Sigma^+$ states. The reason is that this order is unambiguous and does not depend on the surface on which CO is adsorbed.

In the next section we give a summary of the model and the details of the method of calculation of the cross section. The cluster calculations are standard and the backscattering method have been presented in a preceding paper (BBR). Section III presents the results of the calculations and compares them to the experimental data. Section IV discusses the obtained results and summarizes our findings.

II. SUMMARY OF THE METHOD AND THE DETAILS OF THE CALCULATION

The study of photoionization of adsorbates requires measurements and calculations of the differential cross section. The expression of the cross section is usually written in laboratory frame defined with the *z* axis perpendicular to the surface. In our physical problem, there are three preferential directions (see Fig. 1): the incident direction of light (angles θ_q and φ_q; this direction corresponds to propagation direction for circularly polarized light and to the direction of the polarization vector for linearly polarized light), the direction of the molecular axis of the adsorbate, and the ejection direction of the electron (θ and φ). The CO molecule is normal to the surface; therefore, the laboratory and molecular frames are superposed on each other. In the present paper, concerned with on-top adsorption sites, we represent the molecule-surface interaction by the interaction between the molecule and a single atom of the surface. If the electron is escaping in the direction of the surface [Fig. 1(b)], then it will undergo collisions with the atoms of the metal and will be reflected (backscattered) or refracted by the

surface. As mentioned in the Introduction, we model this phenomenon by a phenomenological step potential (BBR). In the framework described above, the expression of the cross section has been derived by several authors (see Refs. 4–6). The difference between these derivations and the present model is the additional term originating from backscattering of electrons. The detailed derivation was given in BBR and the final expression of the differential cross section including backscattering reads (atomic units are used in this paper)

$$\frac{d\sigma^{m^{\rm ph}}(\mathbf{k},\Omega_q)}{d\Omega_k}=3\sigma_{\lambda''}(k)\sum_{l_1\lambda_1\lambda_1^\gamma l_2\lambda_2\lambda_2^\gamma}\bar{T}^{\lambda_1^\gamma}_{l_1\lambda_1\lambda''}(k)\bar{T}^{\lambda_2^\gamma *}_{l_2\lambda_2\lambda''}(k)D^{(1)}_{\lambda_1^\gamma m^{\rm ph}}(\Omega_q)D^{(1)*}_{\lambda_2^\gamma m^{\rm ph}}(\Omega_q)Y_{l_1\lambda}(\hat{k})Y^*_{l_2\lambda_2}(\hat{k})\ , \tag{1}$$

where $\Omega_k=\{\theta,\varphi\}$, $\sigma_{\lambda''}=(4\pi^2/3)\alpha E_{\rm ph}B_{\lambda''}$ is the total cross section in the gas phase, α is the fine-structure constant, $E_{\rm ph}$ the photon energy, and $B_{\lambda''}=\sum_{l\lambda\lambda^\gamma}|\langle\psi^f_{kl\lambda}(\mathbf{r})|\hat{T}_{\lambda^\gamma}|\psi^i_{\lambda''}(\mathbf{r})\rangle|^2$ is the sum of squares of the unnormalized transition moments. In (1) $\bar{T}^{\lambda^\gamma}_{l\lambda\lambda''}(k)$ is the normalized transition moment defined below, $D^{(1)}_{\lambda^\gamma m^{\rm ph}}(\Omega_q)$ is the Wigner rotational function connecting the photon and molecular frames (with the convention of active rotations, see, e.g., Zare[26]), and $Y_{l\lambda}(\hat{k})$ the spherical harmonics associated with the momentum of the escaping photoelectron. The normalization transition moment reads

$$\bar{T}^{\lambda^\gamma}_{l\lambda\lambda''}(k)=\frac{\langle\psi^f_{kl\lambda}(\mathbf{r})|\hat{T}_{\lambda^\gamma}|\psi^i_{\lambda''}(\mathbf{r})\rangle}{\sqrt{B_{\lambda''}}}F^*_{l\lambda}(k,\theta)\ , \tag{2}$$

where $\hat{T}_{\lambda^\gamma}$ is the dipole transition-moment operator. The backscattering factor $F_{l\lambda}(k,\theta)$ can be expressed in two ways:

$$F_{l\lambda}(k,\theta)=1+(-1)^{l+\lambda}R(k,\theta)$$

$$=1+\rho(k_z)\exp\{-i[2k_zz_0-\pi(l+\lambda)]\}\ . \tag{3}$$

In (3), the first term corresponds to the direct [(d) in Fig. 1] and the second term to the backscattered [(b) in Fig. 1] electron and $\rho(k_z)$ is equal to $(|k_z|-k_z')/(|k_z|+k_z')$. $F_{l\lambda}(k,\theta)$ and $R(k,\theta)$ are complex numbers, k is the momentum of the electron with $k_z=k\cos\theta$ (see Fig. 1). In the bulk, the z component of the momentum is $k_z'=\sqrt{k_z^2-2mV_0/\hbar^2}$, where $k=\sqrt{2mE/\hbar^2}$, E is the kinetic energy of the electron, m is its mass, V_0 is the inner potential of the solid, and $\hbar$ is the Planck constant. This expression, derived for a step potential,[10] is valid for a structureless surface and low-energy electron that will have the associated wavelength too large to distinguish between the different atoms of the surface. The factor $F_{l\lambda}(k,\theta)$ can be written as a complex number in polar form and one can easily show that the backscattering contribution appears in the module and phase of the transition moment $\bar{T}^{\lambda^\gamma}_{l\lambda\lambda''}(k)$ in a complicated way. The detailed analysis of the direct and backscattering terms for a step potential has been given in BBR.

More general expressions (see, e.g., Refs. 12 and 13), mainly having a smooth variation with z, can be derived. Also one can include the backscattering directly in the calculation of the electronic wave function using a large or imbedded cluster or by solving asymptotically a Schrödinger equation with a modified potential including backscattering. As mentioned in the Introduction, the present model is based on an intermediate two-step procedure. We first calculate a small cluster built from the adsorbate and one atom of the surface, a cluster that takes into account the local chemisorption forces: We then add a step potential to include all the other atoms of the surface that will backscatter the photoelectron.

The CDAD (Refs. 3–6) is the difference between left and right circularly polarized light differential cross sections. One can derive two forms of CDAD:

$$I_{\rm CDAD}=\frac{d\sigma^{+1}(\mathbf{k},\Omega_q)}{d\Omega_k}-\frac{d\sigma^{-1}(\mathbf{k},\Omega_q)}{d\Omega_k}$$

$$=\frac{-3\sigma_{\lambda''}(k)}{\pi}\sum_{l_1\lambda_1\lambda_1^\gamma l_2\lambda_2\lambda_2^\gamma}\delta_{\lambda_1^\gamma,\lambda_2^\gamma+1}d^{(1)}_{-\lambda_1^\gamma-1}(\theta_q)d^{(1)}_{\lambda_2^\gamma 1}(\theta_q)\Theta_{l_1-\lambda_1}(\theta)\Theta_{l_2\lambda_2}(\theta)\sin[(\varphi_q-\varphi)]$$

$$\times|\bar{T}^{\lambda_1^\gamma}_{l_1\lambda_1\lambda''}(k)||\bar{T}^{\lambda_2^\gamma}_{l_2\lambda_2\lambda''}(k)|\sin[(\mu_{l_1\lambda_1}-\mu_{l_2\lambda_2})] \tag{4}$$

and

$$A_{\rm CDAD}=I_{\rm CDAD}\Big/\left\{\frac{d\sigma^{+1}(\mathbf{k},\Omega_q)}{d\Omega_k}+\frac{d\sigma^{-1}(\mathbf{k},\Omega_q)}{d\Omega_k}\right\}\ , \tag{5}$$

where $\delta_{\lambda_1^\gamma,\lambda_2^\gamma\pm1}$ is the Kronecker symbol selecting the molecular symmetries differing by 1, i.e., σ and π; π and δ, etc. The function $d^{(1)}_{\lambda^\gamma m^{\rm ph}}(\theta_q)$ is real and a part of Wigner rotational function, i.e., $D^{(1)}_{\lambda^\gamma m^{\rm ph}}(\Omega_q)=\exp(-i\lambda^\gamma\varphi_q)d^{(1)}_{\lambda^\gamma m^{\rm ph}}(\theta_q)\exp(-im^{\rm ph}\chi_q)$. Finally, $\Theta_{l\lambda}(\theta)$ is a part of the spherical harmonics function

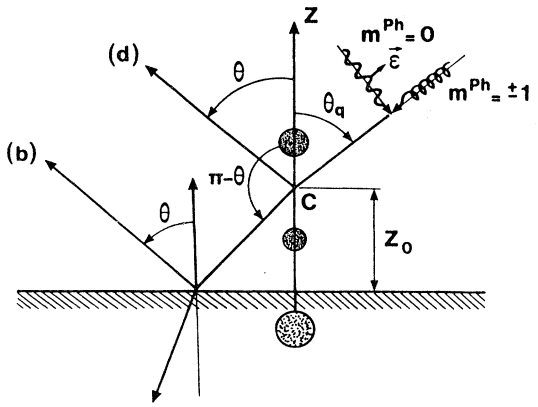

FIG. 1. Backscattering of photoelectrons using a model of a step potential (BBR). The system of coordinates is normal to the surface. Its origin C is located at the center of mass of the adsorbed molecule. The arrows (d) and (b) correspond to direct and backscattered electrons, respectively. The photon is incident with the angles θ_q and φ_q. The standard assumption is made about the z direction of the photon coordinate system: for circularly polarized light ($m^{ph}=\pm1$), the photon spin is parallel to the propagation direction; for linearly polarized light ($m^{ph}=0$), the electric vector is perpendicular to the propagation direction of the photon.

$Y_{l\lambda}(\theta,\varphi)=\Theta_{l\lambda}(\theta)\exp(i\lambda\varphi)/\sqrt{2\pi}$. In (4), the complex transition-moment $\bar{T}^{\lambda\gamma}_{l\lambda\lambda''}(k)$ defined in (2) is expressed in polar form ($|\bar{T}^{\lambda\gamma}_{l\lambda\lambda''}(k)|$, module; $\mu_{l\lambda}$, phase). In expression (5), we have normalized I_{CDAD} to the sum over the differential cross sections corresponding to right and left polarizations. This is very convenient from an experimental point of view because one can hardly obtain absolute CDAD. But, because the two quantities of expression (5) can have very different angular behaviors, this ratio can generate significant distortions. It will be shown in the next section that A_{CDAD} can give spurious peaks that sometimes mask the true angular dependence of I_{CDAD}. The backscattering is hidden here in the transition moments $\bar{T}^{\lambda\gamma}_{l\lambda\lambda''}(k)$ and its relation to CDAD is not explicit. One has to refer to the analytical analysis performed in BBR showing that backscattering will not give qualitatively new contribution to CDAD except if it depends explicitly on azimuthal angle difference $\varphi_q-\varphi$. This is not the case with the present backscattering step potential [see Eqs. (3) and (4)]. However, containing only the $\sigma\pi$ cross term of the differential cross section and depending on the sine of the phase difference of the transition moments, the CDAD can give supplementary information about the mechanism of ionization and the origin of the measured flux of electrons: from the adsorbate or from the bulk metal.

To obtain the transition moment $\langle\psi^f_{kl\lambda}(\mathbf{r})|\hat{T}_{\lambda\gamma}|\psi^i_{\lambda''}(\mathbf{r})\rangle$, we have separately calculated the initial $\psi^i_{\lambda''}(\mathbf{r})$ and final $\psi^f_{kl\lambda}(\mathbf{r})$ wave function. (For details see the calculation of CO photoionization in gas phase.[27–29]) As discussed above, we represent the adsorbed CO molecule by a linear NiCO cluster. The initial state is bound and it has been obtained at the self-consistent-field (SCF) level using the Slater basis functions version of the Alchemy-SCF program.[30] The atomic basis set is of $2-\zeta$ quality[31] and it was augmented by unoptimized polarization basis functions[32] ($3d$ functions for C and O atoms having the exponents 1.582, 1.238, and 1.913, 1.636, respectively; $4d$ functions for Ni atoms having the exponents 2.5 and 1.5) and diffuse s and p functions located at the center of mass of the NiCO cluster [$3s$ and $4s$ with the quantum defect 0.94, $3p\sigma$ and $4p\sigma$ with the quantum defect 0.58, and finally $3p\pi$ and $4p\pi$ with the quantum defect 0.68 (Ref. 27)]. Following Kao and Messmer,[33] see also Dubs, Smith, and McKoy,[5] we choose the ground state of NiCO to be $^1\Sigma^+$ state with Ni corresponding to the $3d^{10}$ configuration. This electronic configuration corresponds to $Ni(CO)_4$ cluster ground state and better describes the σ donation and π backdonation processes as compared to $3d^9 4s^1$ stable configuration of the Ni atom. In the present work we use the $Ni(CO)_4$ geometry, namely 3.471 and 2.173 a.u. for Ni-C and C-O bonds. The CO bond distance is slightly larger than the value used in BBR but does not influence significantly the results presented here.

In Table I we display the SCF energies for different atomic basis sets of the initial state $\psi^i_{\lambda''}(\mathbf{r})$ (corresponding to the state $^1\Sigma^+$) of the NiCO cluster. As expected, all the present SCF energies obtained with Slater-type basis sets are lower than those obtained using Gaussian-type basis sets.[34] Comparing the energy levels of CO and NiCO and using the results of population analysis related to the bond character of orbitals, we have made the following identification: 4σ, 1π, and 5σ orbitals of CO correspond to 9σ, 3π, and 10σ orbitals of NiCO. This assignment is in agreement with the one given by Dubs, Smith, and McKoy.[5] As mentioned in the Introduction, we will continue to use for different orbitals the labels of the gas-phase CO molecule.

The final-state wave function $\psi^i_{\lambda''}(\mathbf{r})$ is calculated in the frozen-core static-exchange (FCSE) approximation by the method developed by one of us.[28] The molecular basis is the same as the one used for the initial state. (see Table I). To calculate explicitly the continuum electron wave function, we first use a one-center expansion of molecular orbitals and build the corresponding one-center $N-1$ electrons potential. Then, we solve numerically a close-coupling system of equations.[28,35] Our method includes exchange exactly and consists in a transformation of the original system of integrodifferential equations (integrodifferential because of electron exchange) in a larger system of differential equations where the additional equations correspond to the unknown exchange integral. (See the original method by Hartree[36] efficiently adapted for molecules by one of us.[35]) To handle a system of equations of reasonable size, one should limit the number of terms in the expansion of the potential, bound orbitals, and exchange interaction functions. We have chosen the following maximum values for the expansions: $l=10$ for the expansion of continuum function, $l_b=30$ for the bound electron, $\gamma_{\mathrm{st}}=50$ for the electron-electron interaction, and $\gamma_{\mathrm{ex}}=4$ with $l=10$ and $l_b=10$ for the exchange interaction. The crucial point concerns the exchange because the number of the corresponding equa-

TABLE I. Atomic and molecular basis functions and SCF energies of the NiCO cluster corresponding to the $^1\Sigma^+$ state having $3d^{10}$ electronic configuration.

Name	Atomic basis set	SCF energy (a.u.)	Molecular basis set for FCSE
$(2-\zeta)$	Slater double-ζbasis set (Refs. 31 and 32)	−1619.2311	$11\sigma 4\pi$
$(2-\zeta+\text{diff})$	Slater double-ζ and diffuse $3s$ and $3p$ at the center of mass of NiCO	−1619.2336	$11\sigma 4\pi$
$(2-\zeta+\text{pol})$	Slater double-ζ and polarization functions $3d$ for C and O and $4d$ for Ni atoms	−1619.4115	$11\sigma 4\pi$
$(2-\zeta+\text{pol}+\text{orth})$	Same atomic basis as $(2-\zeta+\text{pol})$	−1619.4115	$12\sigma 5\pi$[a]
$(2-\zeta+\text{diff}+\text{pol})$	Combination of $(2-\zeta+\text{diff})$ and $(2-\zeta+\text{pol})$ bases	−1619.4120	$11\sigma 4\pi$
$(2-\zeta+\text{diff}+\text{pol}+\text{orth})$	Same atomic basis as $(2-\zeta+\text{diff}+\text{pol})$	−1619.4120	$12\sigma 5\pi$[a]
(Gauss)	Gaussian double-ζ with diffuse and polarization functions (Ref. 5)	−1618.7383	$11\sigma 4\pi$

[a]The first two valence virtual molecular orbitals are used in the orthogonalization procedure when calculating the FCSE continuum electron wave function (see text).

tions rises rapidly with γ_{ex}. For the maximum of the $(4\sigma)^{-1}$ shape resonance, we raise γ_{ex} to 10, with $l_b=10$ and $l=10$, without significant difference in the photoionization differential cross section. The need of few exchange functions in our method is probably related to the flexibility of these functions that are recalculated for each kinetic energy of the electron.

In the FCSE equations, one usually introduces an orthogonalization constraint between the continuum and discrete functions of the same symmetry (see, for example, Burke, Chandra, and Gianturco[37]). This constraint is usually restricted to the occupied molecular orbitals but can be extended, as it was done for the gas-phase continuum function of CO (see, e.g., Lucchese and McKoy[34]), to the low-lying-valence virtual orbitals. In the case of NiCO, the reason for such an extended orthogonalization is that for σ symmetry the energy of the $4s$ virtual orbital of Ni is very close to that of $3d$ (In other words, the $3d^{10}$ and $3d^9 4s^1$ configurations are very close in energy, see above). For the π symmetry this orthogonalization eliminates the $2\pi^*$ orbital (having CO molecule character) from the low-energy region of the shape resonances. In the language of electronic configuration interaction, the valence virtual orthogonalization discussed above corresponds to inclusion in the calculations of the monoexcited configurations. From the point of view of molecular-orbital theory, a shape resonance corresponds to an antibonding molecular virtual orbital having its energy in the region of shape resonances. The orthogonalization procedure consists precisely in inclusion of some virtual-orbital antibonding character in the continuum function and shifting the virtual orbital to higher energies. The different molecular basis sets, including valence virtual orbitals, are also presented in Table I. In the calculation of the differential cross section, we have used the ionization potentials corresponding to the Ni(111) surface taken from Williams *et al.*,[38] respectively, of 13.5, 11.95, and 16.5 eV for 5σ, 1π, and 4σ ionizations. We have taken the work function equal to 4.85 eV.

In our simple physical model, based on the reflection of the electron on a step potential representing a structureless surface, we locate the step potential at the distance z_0 from the center of mass of the CO molecule (Fig. 1). This step represents an effective plane whose position is determined by the interaction of the photoelectron with the electrons and atoms of the surface. The inner potential $V_0=-12.5$ eV corresponds to a surface of Ni(111) (see Nagano *et al.*[9] and also BBR). The distance z_0 is viewed as a phenomenological parameter and to fix its value we first calculate the cross section as function of z_0 and kinetic energy of the electron for an incident linearly polarized light at $\theta_q=45°$, a normal ejection of the electron ($\theta=0$), and a zero azimuthal angle difference ($\phi_q-\phi=0$). We have also fixed the Ni-C and CO internuclear distances to 3.471 and 2.173 a.u., respectively, in agreement with low-energy-electron-diffraction and electron-energy-loss-spectroscopy measurements.[39] Therefore, the only varying distance is z_0 between the center of mass of CO and a fictive plane of the step potential. This distance was varied between 1.5 and 5.5 a.u. two extreme values either close to the C atom or located in the bulk. The calculations were done with the basis set $(2-\zeta\text{diff}+\text{pol}+\text{orth})$ of Table I and the results are presented in Fig. 2. The direct (d) and backscattered (b) waves interfere giving, depending on the distance z_0 and the wavelength of the electron, constructive or destructive interference. The best fit with the experimental data is obtained for $z_0=4$ a.u. We neglected the refraction effects at the surface barrier because, at least for normal emission (BBR), these effects are not too important. We have also neglected the inner potential corresponding to the CO overlayer, a reasonable approximation for the low-coverage experiments discussed here. As the experimental photoionization cross section is not given in absolute units, the above choice will mainly influence the branching ratio between 5σ and 4σ excitation channels.

III. RESULTS

In this section we present the photoionization differential cross section and CDAD in the region of 4σ

and 5σ shape resonances. The calculations correspond to two experimental arrangements with the linearly polarized light: incident angle $\theta_q=45$ about the normal to the surface, normal ejection of the photoelectron ($\theta=0$), and

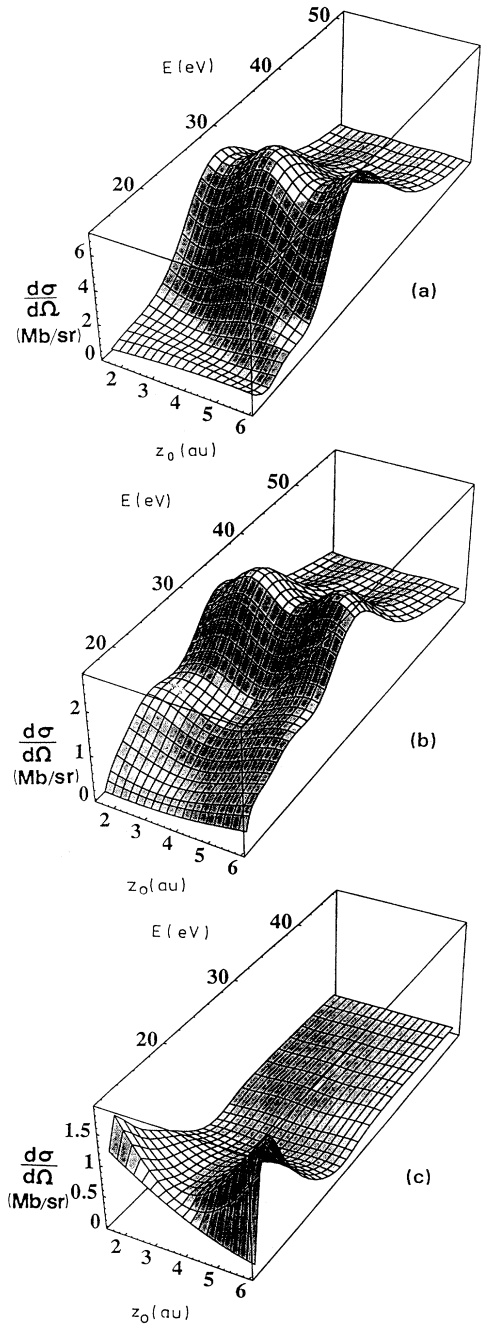

FIG. 2. Differential photoionization cross section as a function of the distance z_0 (z_0 is the distance between the center of mass of the CO molecule and the location of the step potential) and photon energy. The distances between the different atoms are kept fixed (see text). The light is linearly polarized ($m^{\mathrm{ph}}=0$) and the angles with respect to surface normal are $\theta_q=45°$, $\theta=0°$, and $\varphi_q-\varphi=0°$. (a) $(5\sigma)^{-1}$ ionization channel; (b) $(4\sigma)^{-1}$ ionization channel, (c) $(1\pi)^{-1}$ ionization channel.

the azimuthal angle difference $\varphi_q-\varphi$ equal to 0°; incident angle $\theta_q=90$ (s polarization), $\theta=45°$, and $\varphi_q-\varphi=0°$. A third experimental set up was used for CDAD: circularly polarized light with $\theta_q=45°$ and azimuthal angle difference of $\varphi_q-\varphi=45°$. The first question we asked ourselves concerns the influence of the atomic and molecular basis set and backscattering on the resulting differential cross section. This analysis was done using the first geometrical set up. In Fig. 3, we present calculations of the photoionization cross section for the ejection angle of the electron normal to the surface ($\theta=0°, \varphi_q-\varphi=0$) and study its sensitivity to different basis functions sets used in the *ab initio* calculation (see Table I). There are some changes in the intensity at the maximum of the photoionization cross section but qualitatively the shape of this cross section is the same for all the calculations presented in Fig. 3. The essential ingredient in the atomic basis function set are the d atomic polarization functions. This is in contradiction with Lucchese and McKoy[34] and Dubs, Smith, and McKoy[5] who consider that diffuse functions are essential for an accurate calculation. If one adds to the $2-\zeta$ atomic basic only diffuse functions [Table I, ($2-\zeta$+diff), not presented in Fig. 3] without orthogonalization to the valence virtual orbital, then one obtains cross sections that are different from the ones presented in Fig. 3. A qualitative agreement with these graphs is reached provided one orthogonalizes the wave function of the continuum electron to all bound orbitals and the first valence virtual one. In the preceding section, we discussed in detail the origin of the procedure that suggested the orthogonalization of the continuum function and valence virtual orbital. From our discussion, one see that its use is an essential ingredient that stabilizes the cross section. The results presented in Fig. 3 are in good qualitative agreement with Dubs, Smith, and McKoy[5] and very different from the one presented in BBR even including backscattering. In the calculations of Dubs, Smith, and McKoy[5] the 4σ and 5σ excitation channels are of nearly equal intensity. In our calculations, the $(4\sigma)^{-1}$ channel is weaker than the $(5\sigma)^{-1}$ one and results in better agreement with the experimental data. The main difference between the calculations of Dubs, Smith, and McKoy[5] and ours is the atomic basis set of Gaussian type in the first case and of Slater type in the second case. We do not believe that this change of the atomic basis set can explain the difference in the cross sections. This is probably due to orthogonalization to valence virtual orbitals of σ and π symmetry and to photoelectron backscattering. For the $(4\sigma)^{-1}$ channel (Fig. 3), there is a secondary maximum appearing around 25 eV, a maximum that was never obtained in a theoretical calculation before but seems to appear in the experimental results. This maximum is probably a result of an implicit interaction between $5\sigma\rightarrow\varepsilon\sigma$ and $4\sigma\rightarrow\varepsilon\sigma$ shape resonances, an interaction obtained through orthogonalization procedure to the occupied and virtual orbitals in the FCSE calculation. The orthogonalization to the first valence orbital modifies the height of the maximum of the shape resonances (diminish 5σ by about 1 Mb/sr but leave 4σ nearly unchanged) changing the branching ratio between 4σ

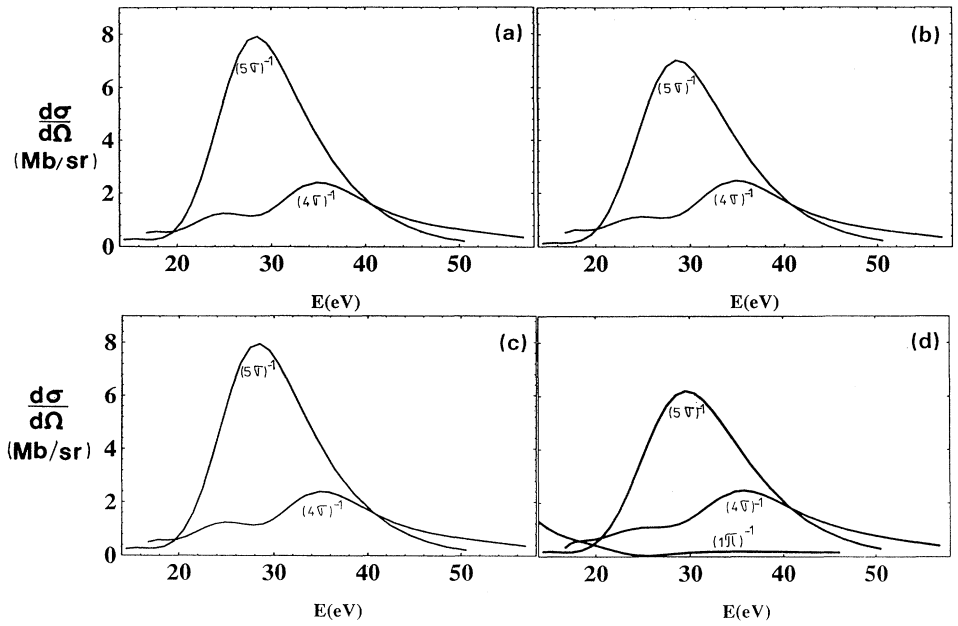

FIG. 3. Photoionization differential cross section of NiCO cluster in the region of the shape resonances as a function of photon energy. The light is linearly polarized ($m^{ph}=0$) and the angles are the same as in Fig. 2. (a), (b), (c), and (d) correspond, respectively, to calculations with the molecular basis ($2-\zeta$+pol), ($2-\zeta$+pol+orth), ($2-\zeta$+diff+pol), and ($2-\zeta$ +diff+pol+orth) (see Table I). In (d) we have also represented the excitation from 1π channel.

and 5σ cross sections. Cross sections including backscattering have not been plotted in Fig. 3 but will be displayed in Fig. 9 when comparing our results to the experimental spectra. The strong influence of orthogonalization on the 5σ excitation channel can be explained as follows. In a free CO molecule, the 5σ orbital corresponds to a lone pair located on the C atom. At adsorption, 5σ interacts not only with occupied $3d$ but also with low-lying virtual $4s$ orbitals of Ni atom (see discussion preceding section) and the lone pair is deplaced towards the O atom. These interactions justify the orthogonalization to $3d$ and $4s$ orbitals, which also acts as local backscattering of electrons. The backscattering from the whole surface is obtained when adding out step potential.

In Figs. 4 and 5, we present a polar plot of the differential cross section at the maximum of the 5σ and 4σ shape resonances (29.5 and 35.8 eV) discarding backscattering and using the same molecular basis sets as in Fig. 3. We display the differential cross section towards the vacuum (the upper-half plane of the figure) as well as the one corresponding to refraction/absorption (lower-half plane of the figure) by the metal. The refracted electron cannot be measured experimentally but, until backscattering is introduced, we keep it for reference to have an idea of the penetration direction of the electron in the metal. The angular behavior of the 5σ shape resonance, obtained using the oriented-in-space model of the CO molecule calculated in BBR, is very different from the one obtained here. Owing to the electrons of the Ni atom, particularly $4s$, the photoelectron is now mainly ejected towards the vacuum even in the case 5σ excitation channel. If the polarization functions are present, the effect of adding diffuse functions is minor. [Compare 4(a) and 5(a) with 4(c) and 5(c), or 4(b) and 5(b) with 4(d) and 5(d) in Figs. 4 and 5.] Angular analysis at the maximum of the resonances confirms the conclusion reached for normal emission: the orthogonalization including the first valence virtual orbitals changes the ratio between 4σ and 5σ intensities, namely, it diminishes the first and enhances the last. In Fig. 4(e), we have represented for reference the ionization from $(1\pi)^{-1}$ channel at 29.5 eV. Except at threshold [see Fig. 3(d)], this channel is very weak and its angular behavior is very different from σ excitation channels and dominated by $\varepsilon\pi$ continuum with a major contribution from the $d\pi$ wave.

In Fig. 6, we present the angular behavior at the maximum of our shape resonances discarding (dotted line) or including (full line) backscattering of the electron by the surface. As in Figs. 4 and 5, and for the same reasons, we display also the photoelectron intensity towards the bulk. For 5σ excitation, the backscattering displaces the lobe of the differential cross section to larger angles but the intensity is not changed in a significant way. The initial 5σ orbital is located close to the surface and it participates to the adsorbate-metal bond. The reorganization of the 5σ electronic cloud due to the presence of the Ni atom in our model cluster, penetration and backscattering are already taken into account in the direct term of the transition moment (2). This explains the relatively weak influence of the photoelectron backscattering second term. We have also identified that the angular displacement of the resonance maximum is due to electron exchange related to π electrons. The 4σ orbital does not participate to the above-mentioned bond and it is located at the oxygen end, i.e., farther from the backscattering step potential. This difference in location and participation in the bond with the metal explains the difference in the influence of the backscattering on the differential cross sections clearly appearing on Figs. 6(a) and 6(b).

In Figs. 7 and 8, we present the differential cross section for circularly polarized light [$m^{ph}=+1$ and $m^{ph}=-1$; Figs. 7(a) and 8(a), and 7(d) and 8(d)], the unnormalized circular dichroism in the angular distribution [I_{CDAD} Eq. (4); Figs. 7(b) and 8(b), and 7(e) and 8(e)], and

normalized one [A_{CDAD} Eq. (5); Figs. 7(c) and 8(c), 7(f) and 8(f)] at the maximum of the shape resonances. The two columns correspond to discarding and including the backscattering in the model. The differential cross sections, given here for reference, are similar to that for linearly polarized light (Figs. 4 and 5) and, because the incident photon arrives at 45°, show no symmetry with respect to the x or y axis. Because $I_{\mathrm{CDAD}} \sim \sin(\theta)$ (Refs. 4 and 6), the Figs. 7(c) and 8(c) display antisymmetric I_{CDAD} about the vertical z axis (i.e., the normal to the surface). The two shape resonances behave very differently: 5σ displays a strong variation with the ejection angle of the electron θ, whereas in the case of 4σ

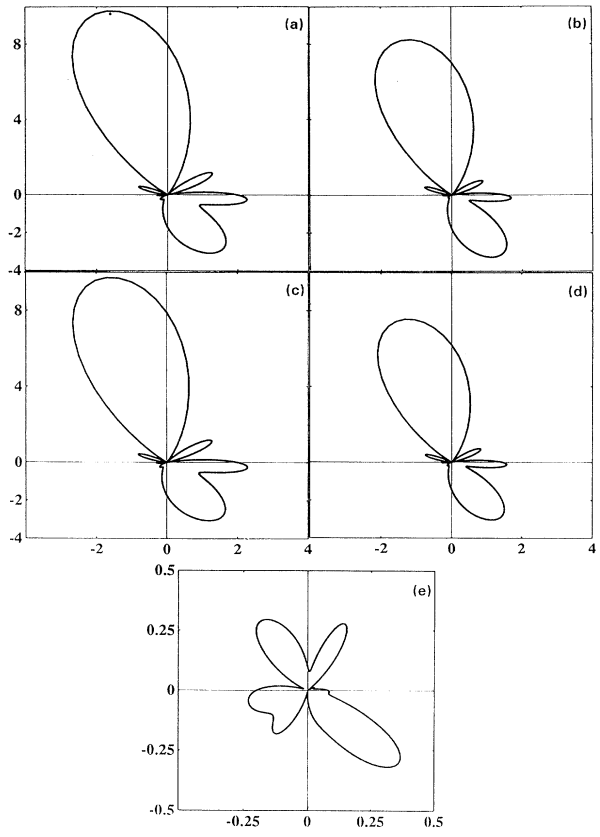

FIG. 4. Polar plots of the differential cross sections of the 5σ and 1π excitations, at the maximum (29.5 eV) of the $(5\sigma)^{-1}$ shape resonance, as a function of θ, the ejection angle of the photoelectron. (a)–(d) correspond to $(5\sigma)^{-1}$ excitation whereas (e) corresponds to the $(1\pi)^{-1}$ excitation. The light is linearly polarized ($m^{\mathrm{ph}}=0$), the incident angle of the photon polarization is $\theta_q=45°$, and $\varphi_q-\varphi=0°$. The differential photoionization cross section has the amplitude that is a point in the xy plane of the page. The $\theta=0$ corresponds to a positive vertical axis and the surface is represented by a plane having as a projection the horizontal axis. For the right-hand side of the graph, $\varphi=0°$, and the left-hand side, $\varphi=180°$. The backscattering is discarded and consequently we display the intensity towards the bulk. (a), (b), (c), and (d) have been calculated, respectively, with the molecular basis sets $(2+\zeta+\mathrm{pol})$, $(2-\zeta+\mathrm{pol}+\mathrm{orth})$, $(2-\zeta+\mathrm{diff}+\mathrm{pol})$, and $(2-\zeta+\mathrm{diff}+\mathrm{pol}+\mathrm{orth})$ (see Table I).

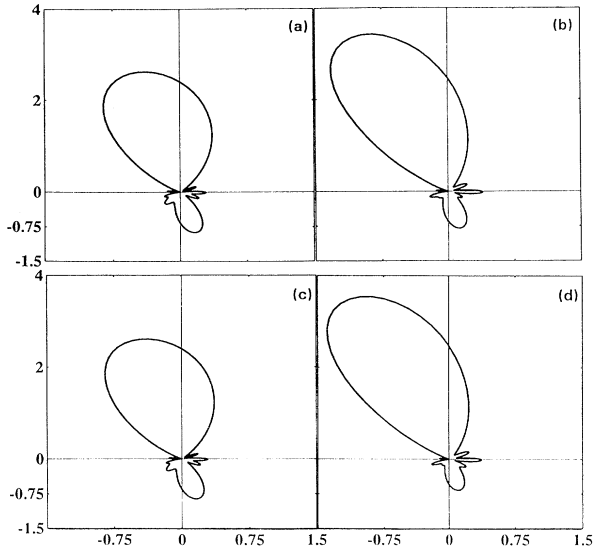

FIG. 5. Polar plots of the differential cross section of the 4σ, at the maximum (35.8 eV) of the $(4\sigma)^{-1}$ shape resonance, as a function of θ, the ejection angle of the photoelectron. The same two-dimensional representation, photon incident angles and polarization, and correspondence between the molecular basis and graphs as in Fig. 4.

there are only two lobes towards the vacuum. This difference cannot be inferred from the differential cross section and is related to the cancellation of many contributions of same sign appearing in the cross section that are absent from CDAD. Now if one calculates A_{CDAD} instead of I_{CDAD} [see Eqs. (4) and (5) of the preceding section and Figs. 7(c) and 7(f), and 8(c) and 8(f)], a quantity usually measured in the experiments, one observes a dramatic change in the angular behavior that is not antisymmetric anymore with respect to the surface normal (z axis). Obviously this is related to the definition of A_{CDAD} as a ratio between an antisymmetric term, displayed in Figs. 7(b) and 8(b), and 7(e) and 8(e), and a nonsymmetric term [the sum of two graphs displayed in Figs. 7(a) and 8(a), and 7(d) and 8(d). To understand this

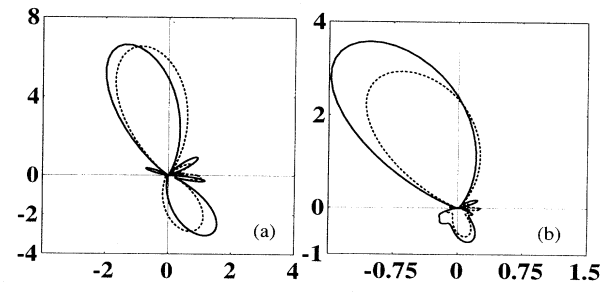

FIG. 6. Polar plots of $(5\sigma)^{-1}$ (a) and $(4\sigma)^{-1}$ (b) excitations discarding (dashed line) or including (full line) backscattering. The molecular basis set $(2-\zeta+\mathrm{diff}+\mathrm{pol}+\mathrm{orth})$ was used in the calculations. Same two-dimensional representation, photon incident angles, and polarization as in Fig. 4. For reference, we display also the lobe towards the bulk (see text).

behavior, a detailed analytical analysis, related to the photon frame transformation, can only be done in the framework of the CDAD formulation of Cherepkov and Kuznetsov[4] or Raseev.[6] This analysis shows that the asymmetry in the denominator of A_{CDAD} appears due to a part of the $\sigma\pi$ interference term of the cross section different from the one associated to I_{CDAD}. Finally the backscattering changes [Figs. 7(e) and 7(f), and 8(e) and 8(f)] the amplitudes of different lobes in the case of 5σ channel but modifies only slightly 4σ one. As discussed in BBR, the structureless step potential used to simulate backscattering does not depend on azimuthal phase difference $(\varphi_q-\varphi)$ and consequently can only change the amplitude of CDAD lobes. (See, also, the next section.)

Let us now turn to the comparison with the experiment. In Figs. 9 and 10, we present the differential cross section for two geometrical set ups. In Fig. 9, the linearly polarized light is incident at 45° and the electron is escaping normal to the surface. This geometry does not correspond to strict selection rules of oriented-in-space molecules discussed by Plummer and Eberhardt[14] but the ejection of the electron normal to the surface favors the σ excitation. The best (2−ζ+diff+pol+orth) molecular basis was used in the calculation and the ionization and inner potentials correspond to Ni(111) surface (Ref. 38, see preceding section). We have plotted our theoretical results of the linear NiCO cluster together with the experimental results for Ni(111) (first column) and Ni(100) (second column) surfaces.[40,41,14] The theoretical model corresponds to the on-top CO molecule adsorbed normal to the surface having axial symmetry. For Ni(111) and Ni(100) surfaces, the adsorption site corresponds to a C_6 and C_4 local-symmetry axis, respectively. Obviously, the C_6 axis is closer to the axial symmetry we use in our model. One sees that the experimental and theoretical results of the first column of Fig. 9 are in better agreement with each other that those of the second column. Note particularly the inversion of the branching ratio [Fig. 9(c)] of 5σ as compared to the 4σ channels that appear in the theoretical as well as in the experimental [Ref. 14 (p. 626)] results. One should also note a larger discrepancy near the photoionization threshold. This is probably due to the presence of electronic autoionizations in this region and may be related to the $2\pi^*$ low-lying unoccupied orbital.

In Fig. 10, the forbidden-geometry experimental set up

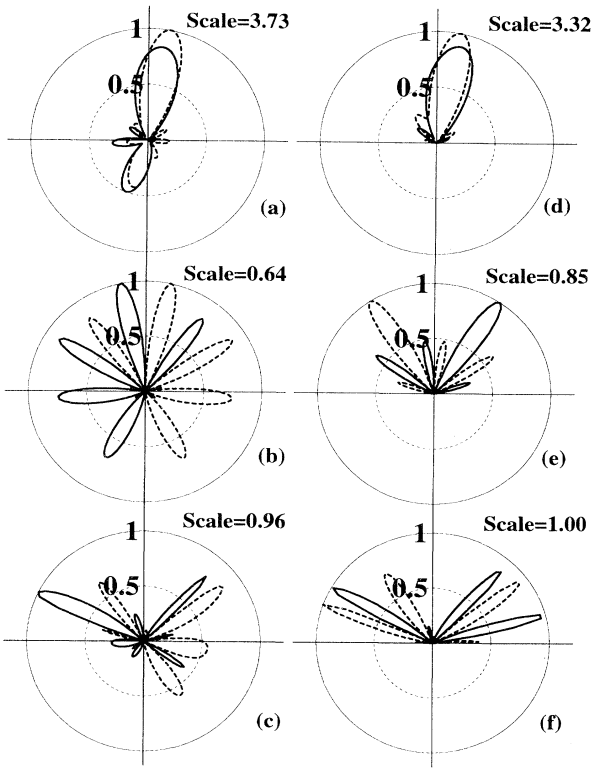

FIG. 7. Polar plot of differential cross section and CDAD at the maximum of the 5σ shape resonance. The molecular basis set (2−ζ+diff+pol+orth) was used in the calculation. The photon is circularly polarized with the incident angle $\theta_q=45°$ and $\varphi_q-\varphi=45°$. The maximum value of the cross section is taken as unity and the scale factor given in the figure relates this amplitude to the actual one. The calculations in the first column discard backscattering; those in the second one include it. (a) and (d) correspond to the differential cross sections for $m^{\mathrm{ph}}=1$ (full line) and $m^{\mathrm{ph}}=-1$ (dashed line); (b) and (e) to the absolute CDAD [I_{CDAD} of Eq. (4)]; and (c) and (f) to the normalized CDAD [A_{CDAD} of Eq. (5)]. In the CDAD graphs, full curves correspond to a positive dichroism, whereas the dashed curves correspond to the negative dichroism.

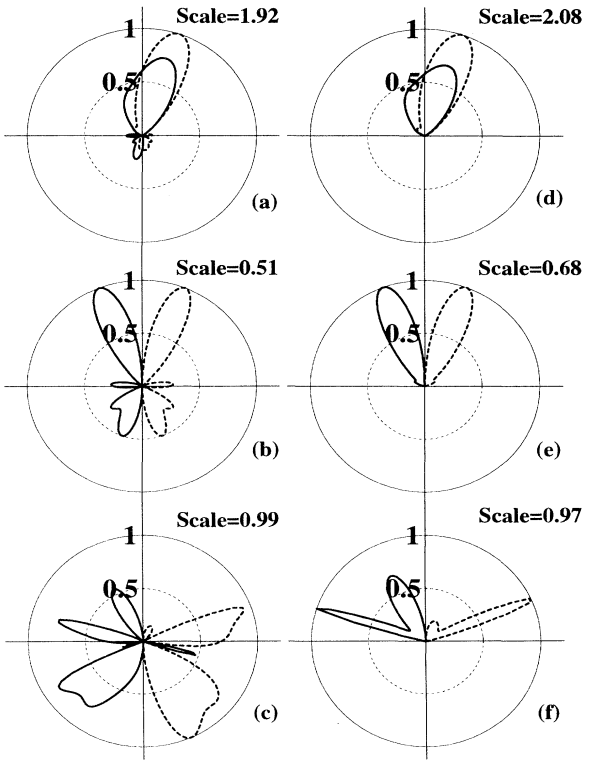

FIG. 8. Polar plots of differential cross section and CDAD at the maximum of the 4σ shape resonance. Same captions as in Fig. 7.

(s-polarized light) was used that discards the $\sigma-\sigma$ excitation. Therefore, the resonant $\varepsilon\sigma$ continuum cannot be reached by the excitation of 5σ and 4σ channels. However, for experimental data corresponding to both Ni(111) [Fig. 10(a)] and Ni(100) [Fig. 10(b)] surfaces, one sees a resonance in the energy region of the 5σ excitation channel. The usual explanation of this abnormal intensity is related to ionization from 1π that have an ionization potential close to that of 5σ orbital. The allowed excitations are now $1\pi\rightarrow\varepsilon\sigma$, $\varepsilon\delta$. (The forbidden excitation for this orbital is $1\pi\rightarrow\varepsilon\pi$.) But, the transition probability to these channels is very low. (See the discussion in gas phase by Leyh.[42]) In fact, the theoretical calculations for 1π ionization [see the amplitude of $(1\pi)^{-1}$ in Figs. 3(d) and 5(e)] show a weak cross section with a nonresonant structure near the threshold and a flat behavior between 30 and 40 eV that cannot explain the feature seen in the experimental spectrum of Fig. 10. The experimental cross section was measured for an ejection angle of the electron of 45° that does not correspond to the forbidden geometry for excitation to either $\varepsilon\sigma$ or $\varepsilon\pi$ continuum. But the $\varepsilon\sigma$ shape resonance will be very weak and the enhancement in the cross section, appearing at higher energy (40 eV compared to 36 eV in Fig. 9), can be related to an unknown $\varepsilon\pi$ shape resonance. Let us comment further on this $\varepsilon\pi$ shape resonance appearing in the 5σ excitation channel. First, we have verified that there is a strong variation in the eigenphase of the final continuum electron wave function corresponding to the $\varepsilon\pi$ continuum. This variation corresponds to a 0.60π jump and appears in the p, d, f, and h partial waves around 40 eV. It can be associated to a εd resonance known to appear in the $\varepsilon\pi$ continuum in e-molecule collisions.[43] One can verify that an $\varepsilon\pi$ structure is really present in the photoionization spectrum also by looking at the angular distri-

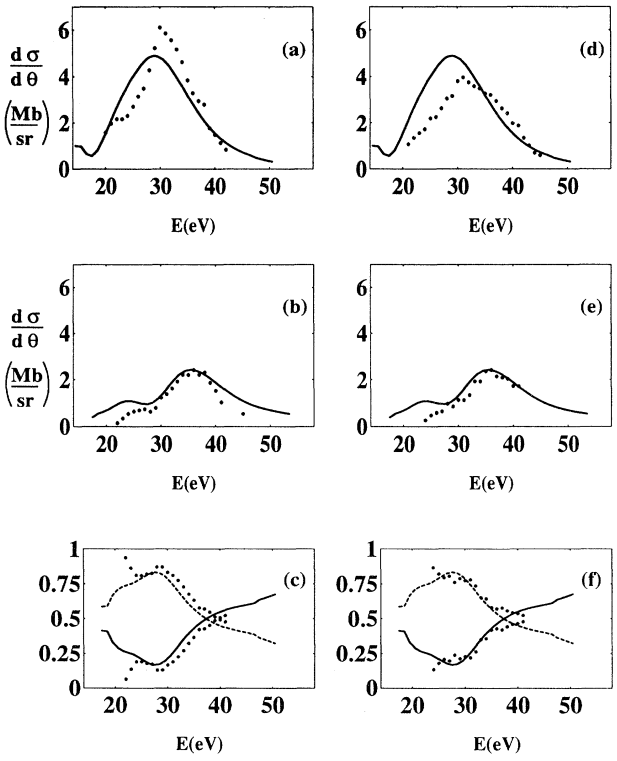

FIG. 9. Photoionization differential cross section including backscattering compared to the experimental data. The molecular basis set $(2-\zeta+\text{diff}+\text{pol}+\text{orth})$ was used in the calculations. The incident angle of the linearly polarized photon is 45° with $\varphi_q=\varphi=0°$ and the ejection angle of the electron is 0°. The two columns of the figure display the same theoretical data obtained using normal to the surface NiCO cluster and the experimental geometry. In the first column, the experimental points are for CO on Ni(111) taken from Plummer and Eberhardt (Ref. 14) (the experiments were performed by Allyn in his Ph.D thesis) and in the second column those for CO on Ni(100) (Refs. 40 and 41). The first line corresponds to the 5σ ionization channel [(a) and (d)], the second line to the 4σ channel [(b) and (e)], and the last line to the branching ratio [(c) and (f)]. The upper curve in (c) and (f) corresponds to the theoretical branching ratio of cross sections $(5\sigma+1\pi)/(5\sigma+1\pi+4\sigma)$, whereas the lower one to the $4\sigma/(5\sigma+1\pi+4\sigma)$.

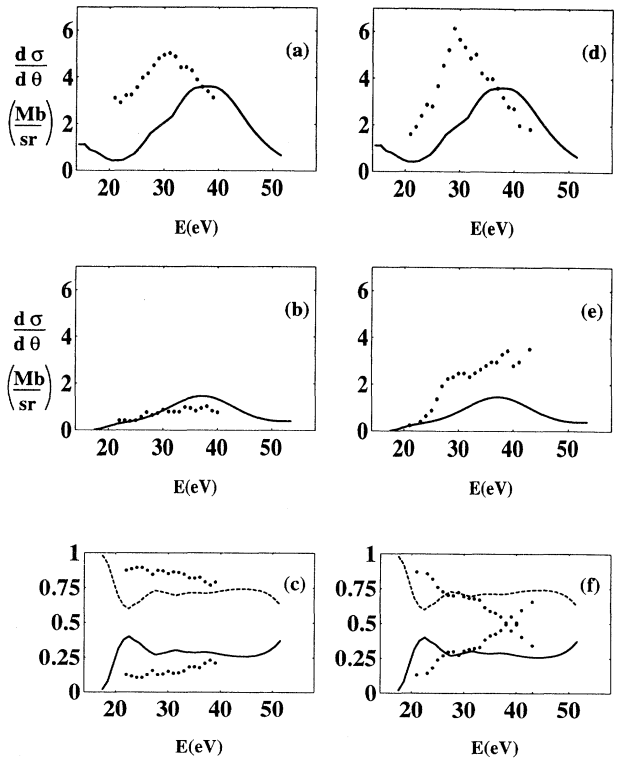

FIG. 10. Photoionization differential cross section including backscattering compared to the experimental data. In the experimental set up, the incident angle of the linearly polarized photon is $\theta_q=90°$ (s polarization) and the ejection angle of the electron is 45°. The theoretical calculations correspond to the same polarization but the electron ejection angle is 30° and $\varphi_q-\varphi=0°$ (see text). In the first column, the experimental points are for CO on Ni(111) taken from Plummer and Eberhardt[14] (the experiments were performed by Allyn in his Ph.D thesis), and in the second column, those for CO on Ni(100) (Ref. 14 same reference as above). Same captions as in Fig. 9.

bution of the ejected electrons presented in Fig. 11. This distribution is characteristic for a $d\pi$ orbital. Turning now to the 4σ ionization channel, one sees experimentally a weak resonant structure around 40 eV at least for the CO on Ni(100) surface [Fig. 10(e)]. If real, this structure should also be related to the $d\pi$ shape resonance.

Plummer and Eberhardt[14] have presented the experimental spectrum of Fig. 10 as appearing because the CO molecule adsorbed on-top on Ni-surface is tilted with respect to the normal to the surface. The analysis of experimental data[21,22] usually concludes that the uncertainty in the angle estimation is of the order of 15°. The present model does not permit the calculation of a bent NiCO cluster. The uncertainty in the experimental results, corresponding to nonzero tilt angle, can be simulated by choosing an ejection angle of the photoelectron of the 30° (45°–15°) instead of the experimental one of 45°. The comparison between theory and experiment presented in Fig. 10 is much less convincing than for Fig. 9. One of the reasons can be that the ionization potentials used in our calculation correspond to normal emission of the electron and they will change for 45° because there is a dispersion in **k** vector originating from the surface.

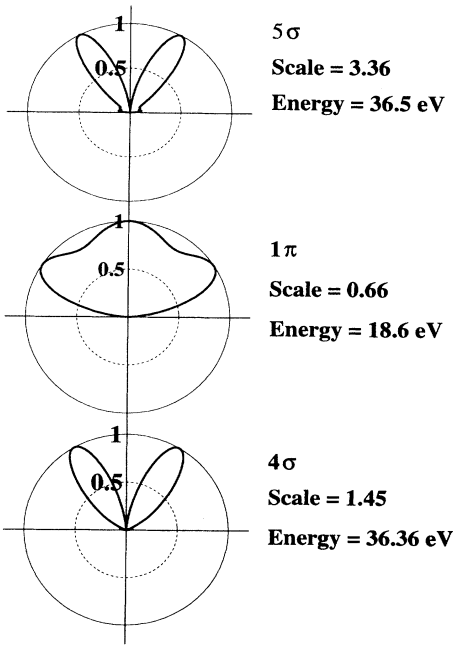

FIG. 11. Polar plots of differential cross section at the maximum of the $\varepsilon\pi$ continuum shape resonance corresponding to 5σ and 4σ excitation channels. The energy of the 1π excitation channel was chosen at the maximum of the corresponding structure in the cross section. The molecular basis set (2−ζ+diff+pol+orth) was used in the calculation. The maximum value of the cross section is taken as unity and the scale factor given in the figure relates this amplitude to the real one. The photon is linearly polarized with the incident angle $\theta_q = 90°$ (*s* polarization) and $\varphi_q - \varphi = 0°$.

Another reason can be related to the tilt angle of CO molecule about the surface. Even for small tilt angles, the $\sigma \rightarrow \varepsilon\sigma$ transition is allowed and generates a strong mixing between $\varepsilon\sigma$ and $\varepsilon\pi$ resonances shifting the maximum of the cross section to lower energies. Unfortunately, for the moment, we cannot verify this hypothesis. The above analysis does not apply exactly to the experimental set up of Fig. 9 because the incident angle of the photon is 45°, which does not correspond to a strict selection rule. Even for a linear cluster, both transitions to $\varepsilon\sigma$ and $\varepsilon\pi$ are allowed and the two resonances discussed above merge in a single structure in the experimental spectrum. Finally, as explained for allowed geometry cross section (Fig. 9), the influence of electronic autoionization related with $2\pi^*$ unoccupied orbital cannot be ruled out. In fact this influence should in principle be stronger for present forbidden geometry because it concerns an electronic interaction between $2\pi^*$ orbital and a shape resonance associated with $\varepsilon\pi$ continuum, both having a large contribution from the *d* wave.

The conclusion of the analysis of the results presented in Figs. 9 and 10 shows that it is dangerous to reduce the argumentation in the interpretation of the experimental spectra to the selection rules only.[14] The presence of many resonances in molecular adsorbates, that eventually do not appear in the gas phase, could complicate the simple and elegant analysis based on selection rules. One should remember that from a σ bound orbital two transitions, to $\varepsilon\sigma$ and $\varepsilon\pi$ degenerate continua, are accessible in photoionization; we demonstrate that the transition to $\varepsilon\pi$ continuum usually neglected can explain the features seen in the forbidden-geometry spectrum.

IV. DISCUSSION AND CONCLUSION

Let us discuss in more general terms our model. First there are recent calculations of metallic atom CO molecule clusters by Fournier.[44] He has used a density-functional approach to obtain the energies corresponding to the ground states of NiCO, CrCO, and CuCO clusters as a function of the bending metallic atom-CO angle. The conclusion was that NiCO has a linear structure and this supports our model of on-top CO adsorbed on Ni surfaces. There are also several studies in the literature that calculate a large cluster of metallic atoms (e.g., Ni or Cu) interacting with a single CO molecule,[45,46] but these studies do not consider the photoionization process. They consider the ground state of the cluster and find the stable geometrical configuration which, when reduced to metallic atom-CO molecule cluster, is close to the one considered here. The only photoionization calculations with a large cluster use the X-α multiple-scattering method.[47] But this method is approximated and we think that it is better to calculate at a high level of precision the local interaction between the metallic atom and the CO molecule.

Our cross sections are the first reproducing closely the experiment and our theoretical branching ratios follow the experimental ones at least for normal to the surface ejection of the electrons (see Fig. 9). The agreement is probably due to the orthogonalization to the first valence virtual orbital and to electron backscattering introduced

in our model. The experimental spectra of CO adsorbed on metallic surfaces show an enhancement of 5σ shape resonance, whereas the cross section of 4σ and 1π excitations are only slightly perturbed by it. One explains (Ref. 48, see the Appendix) that the two 5σ and 4σ orbitals mix and give rise to a shifting of the electron density towards the oxygen end of CO, which affect mainly the 5σ excitation. The qualitative explanation given by Greuter *et al.*[48] is verified theoretically by comparing our Figs. 6(a) or 7(a) and Fig. 7 of BBR both displaying the angular behavior of $(5\sigma)^{-1}$ excitation. One really sees the shift of the electron density towards the oxygen end. From the above discussion, one concludes that 5σ excitation is very sensitive to metal-adsorbate interaction and can be used to probe it. Application of the present linear model to CO adsorbed on other surfaces for which there exist experimental results like CO/Al(111),[49] CO/Cu surface,[50] CO/Co(0001),[48] CO/Pt surface,[21] CO/Ir surface,[22] and CO/Fe(110) (Ref. 51) will show if the present model corresponds to an appropriate representation of the adsorbate metal interaction sufficient to reproduce the experimental results particularly for sensitive 5σ excitation.

When we started our calculation of 1π excitation, we knew that for gas-phase CO one calculates a $\varepsilon\sigma$ shape resonance in *e*-ion collisions but not in photoionization.[42] We thought that the perturbation by the metal will give rise to appearance of a shape resonance in photoionization of adsorbed CO. As seen from Figs. 10 and 11 and the discussion in the preceding section, this is not the case. Instead in the forbidden geometry (i.e., *s* polarization) we found that $5\sigma \rightarrow \varepsilon\pi$ transition is responsible for the enhancement in the spectrum. This example shows that restricting the use of the selections rules[14] for oriented-in-space molecules only to known resonances can sometimes be misleading. In experimental work, enhancements of the 5σ cross section in forbidden geometry have been seen not only for the CO/Ni surface[40,41,14] but also by Rieger, Schnell, and Steinmann[21] for CO/Pt(111) and Miranda *et al.*[52] for CO/Pd(111). But, these authors concluded in a nonresonant feature originating from 1π excitation.

As discussed in the preceding section, one should also keep in mind the discrepancy that appears in the branching ratio at threshold in Fig. 9 (allowed geometry) and for all energies in Fig. 10 (forbidden geometry). This discrepancy can possibly be explained by the presence of $2\pi^*$ autoionization or interaction between electronic continua, which will mix the shape resonances associated to the three ionic cores. (See, also, the discussion in BBR.) These interactions, and more generally the electronic correlation, are neglected in our model. Work in this direction, using the method applied to Rydberg autoionizations of oriented-in-space CO molecules,[6] is in progress.

Other phenomena like neutralization are neglected in the present approach but we think that they are unimportant in the case of valence ionization.

We have also shown spectra for CDAD (see Figs. 7 and 8) and their sensitivity to the normalization as defined in Eq. (5). More careful investigation in close relation with the experimentalists is needed to understand how the experiments and calculations should be performed to eliminate the possible origin of spurious effects.

In the present, model backscattering is calculated through a two-step procedure where the transition moment and the backscattering term both fulfill the axial symmetry. For such a model, the backscattering will only lead to quantitative but not qualitative changes in the cross section. Qualitative changes will appear in a two-steps model if the symmetry assumed in the calculation of the direct and backscattering terms is different. In first approximation, the axial symmetry corresponds to molecules adsorbed on on-top sites having high-order local-symmetry-rotation axis. For example, the local-symmetry axis for CO/Ni(111) adsorbate-surface system is C_6. If the direct term is calculated in the axial symmetry approximation and the backscattering term fulfills the local C_6 symmetry, then the sixfold symmetry in the cross section will appear only after including backscattering in the calculation. These considerations are related to the model used and have noting to do with the underlying physics.

The use of a step potential to introduce the backscattering of photoelectrons seems to be a crude approximation that can be justified for low-energy electrons where the associated wave spreads over several atoms. For higher kinetic energies, one should use a formulation where the surface atoms have to be explicitly introduced (see, e.g., Refs. 11 and 54). Moreover, one should include the nuclear motion of the substrate atoms and adsorbate that, particularly in normal emission damp the modulations due to backscattering of electrons emitted in a given direction.[55]

Backscattering played an important role for the oriented-in-space model of CO (BBR) and a secondary role in the linear-cluster model of the present work. Because the chemical bond is weak in physisorbed species, the oriented-in-space model is appropriate for description of these adsorbates. Unfortunately, following Büchner and Raseev,[7] the hindered rotation strongly modifies the calculated purely electronic photionization cross section. For example, for an ejection direction of the electron nearly parallel to the surface, the hindered motion of the internuclear axis can reduce the cross section by as much as a factor of 10 (see, e.g., Ref. 7). This hindered rotation is important for very low coverages where the precession of the adsorbate is nearly free; but, when the coverage is risen to a full monolayer, the precession is stopped by a potential barrier (see, e.g., Ref. 53). One speaks about rigidification that will give rise to an intermediate situation between the oriented-in-space model without nuclear motion and a free precession associated to hindered rotation of a single adsorbed molecule. For chemisorbed species the above-mentioned effects, due to the nuclear motion and neighbors, should be less important. In this case, the chemical bond is strong, the adsorbate is closer to the surface, and the possibility for the adsorbate electron to be delocalized in the bulk significant. For metallic surface, the step potential function is attractive and the electron, instead of being reflected, can easily penetrate in the metal. For physisorbed species located at larger distances from the surface, these effects are

weaker. One should carry detailed calculations on a series of systems to verify the above qualitative discussion.

The present linear model is an approximation to the reality and is appropriate only for photoionization of on-top adsorption sites. As explained above, if the hindered nuclear motion[7] is important and the mean angle between the molecular axis and the surface normal is large, then the model breaks down. Another unfavorable situation appears when one considers bridge sites. These sites have a twofold local symmetry instead of fourfold or sixfold symmetries associated the with on-top sites considered here. For these bridge sites, one should first calculate a model cluster including at least two atoms of the surface; a cluster that, of course, is not linear. We are presently developing a method allowing such a calculation of the transition moments.[56] Then one should generalize the cross-section formula (1) along the lines presented in Refs. 4, 19, and 20. Only after these developments will one be able to answer the question about the influence of the hindered-rotation motion and the adsorption site (on-top or bridge) on the electronic transition moment and cross section.

ACKNOWLEDGMENTS

We are indebted to M. Yoshimine, A. D. Mc Lean, B. H. Lengsfield, P. S. Bagus, and B. Liu for making available the Alchemy II system of programs. P. Budau acknowledges the French government for financial support. We are indebted to M. Büchner and D. Bejan for critical reading of the manuscript and to N. A. Cherepkov for interesting comments.

*Permanent address: Department of Physics, University of Bucarest, P.O. Box MG-11, Bucarest-Magurele, Romania.

†Author to whom correspondence should be addressed. Electronic address: Georges@Raseev.ppm.u-psud.fr

[1]D. Dill, J. Siegel, and J. L. Dehmer, J. Chem. Phys. **65**, 3158 (1976); S. Wallace and D. Dill, Phys. Rev. B **17**, 1692 (1978).

[2]J. W. Davenport, Phys. Rev. Lett. **36**, 945 (1976).

[3]N. A. Cherepkov, Chem. Phys. Lett. **87**, 344 (1982).

[4]N. A. Cherepkov and V. V. Kuznetsov, Z. Phys. D **7**, 271 (1987).

[5]R. L. Dubs, M. E. Smith, and V. McKoy, Phys. Rev. B **37**, 2812 (1988).

[6]G. Raseev, Surf. Sci. **269/270**, 247 (1992).

[7]M. Büchner and G. Raseev, Phys. Rev. B **49**, 2768 (1994).

[8]P. Budau, M. Büchner, and G. Raseev, Surf. Sci. **292**, 67 (1993).

[9]S. Nagano, Z. P. Luo, H. Metiu, W. M. Huo, M. A. P. Lima, and V. McKoy, J. Chem. Phys. **85**, 6153 (1986).

[10]A. Messiah, *Quantum Mechanics* (North-Holland, Amsterdam, 1960), p. 80.

[11]D. Sébilleau, G. Tréglia, M. C. Desjonquère, D. Spanjard, C. Guillot, D. Chauveau, and J. Lecante, J. Phys. (Paris) **49**, 227 (1988).

[12]P. J. Jenning, R. O. Jones, and M. Weinert, Phys. Rev. B **37**, 6113 (1988).

[13]P. T. Leung and T. F. George, J. Chim. Phys. **92**, 226 (1995).

[14]E. W. Plummer and W. Eberhardt, Adv. Chem. Phys. **49**, 533 (1982); C. L. Allyn, Ph.D. thesis, Univ. Pennsylvania, 1978.

[15]H.-J. Freund and M. Neumann, Appl. Phys. A **47**, 25 (1988).

[16]A. M. Bradshaw, in *Structure and Reactivity of Surfaces,* edited by C. Morterra, A. Zecchina, and G. Costa (Elsevier, Amsterdam, 1989), p. 201.

[17]E. Umbach, Appl. Phys. A **47**, 25 (1988).

[18]G. Broden, T. Rhodin, C. Brucker, R. Benbow, and Z. Hurych, Surf. Sci. **59**, 593 (1976).

[19]V. V. Kuznetsov, G. Raseev, and N. A. Cherepkov, Z. Phys. (unpublished).

[20]N. Chandra, J. Phys. B **20**, 3405 (1987).

[21]D. Rieger, R. D. Schnell, and W. Steinmann, Surf. Sci. **143**, 157 (1984).

[22]C. W. Seabury, T. N. Rhodin, M. M. Traum, R. Benbow, and Z. Hurych, Surf. Sci. **97**, 363 (1980).

[23]B. Ritchie, Phys. Rev. A **12**, 567 (1975); **13**, 1411 (1976).

[24]R. L. Dubs, S. N. Dixit, and V. McKoy, Phys. Rev. Lett. **54**, 1249 (1985).

[25]C. Westphal, J. Bansmann, M. Getzlaff, G. Schönhense, N. A. Cherepkov, M. Braunstein, V. McKoy, and R. L. Dubs, Surf. Sci. **253**, 205 (1991).

[26]R. N. Zare, *Angular Momentum* (Wiley, New York, 1988).

[27]B. Leyh and G. Raseev, Phys. Rev. A **34**, 2920 (1986).

[28]R. R. Lucchese, G. Raseev, and V. McKoy, Phys. Rev. A **25**, 2572 (1982).

[29]G. Raseev and L. Machado, in *Half Collision Resonance Phenomena in Molecules,* edited by M. Garcia Sucre, G. Raseev, and S. C. Ross (AIP, New York, 1991), p. 37.

[30]M. Yoshimine, A. D. McLean, B. H. Lengsfield, P. S. Bagus, and B. Liu, Alchemy II system of programs; this is a recent version adapted for workstations.

[31]E. Clementi and C. Roetti, At. Data Nucl. Data Tables **14**, 177 (1974).

[32]A. D. Mc Lean and M. Yoshimine, IBM J. Res. Dev. Suppl. **12**, 206 (1968).

[33]C. M. Kao and R. P. Messmer, Phys. Rev. B **31**, 4835 (1985).

[34]R. R. Lucchese and V. McKoy, Phys. Rev. A **28**, 1382 (1983).

[35]G. Raseev, Comput. Phys. Commun. **20**, 267 (1980); **20**, 275 (1980).

[36]D. Hartree, *The Calculation of Atomic Structure* (Wiley, New York, 1957).

[37]P. G. Burke, N. Chandra, and F. Gianturco, J. Phys. B **5**, 2212 (1972).

[38]P. M. Williams, P. Butcher, J. Wood, and K. Jacobi, Phys. Rev. B **14**, 3125 (1976).

[39]S. Andersson and J. B. Pendry, Phys. Rev. Lett. **43**, 363 (1979); M. Passler, A. Ignatiev, F. Jona, D. W. Jepsen, and P. M. Marcus, *ibid.* **43**, 360 (1979).

[40]C. L. Allyn, T. Gustafsson, and E. W. Plummer, Solid State Commun. **28**, 85 (1978).

[41]C. L. Allyn, T. Gustafsson, and E. W. Plummer, Chem. Phys. Lett. **47**, 127 (1977).

[42]B. Leyh, Ph.D. thesis, Université de Liège, 1986.

[43]W. M. Huo, T. L. Gibson, M. A. P. Lima, and V. McKoy, Phys. Rev. A **36**, 1632 (1987).

[44]R. Fournier, J. Chem. Phys. **98**, 8041 (1993).
[45]C. W. Bauschlicher, Jr. and C. J. Nelin, Chem. Phys. **108**, 275 (1986).
[46]K. Hermann, P. S. Bagus, and C. J. Nelin, Phys. Rev. B **35**, 9467 (1987).
[47]A. Schichel, D. Menzel, and N. Rösch, Chem. Phys. Lett. **105**, 285 (1984).
[48]F. Greuter, D. Heskett, E. W. Plummer, and H. J. Freund, Phys. Rev. B **27**, 7117 (1983).
[49]K. Jocobi, C. Astaldi, P. Geng, and M. Bertollo, Surf. Sci. **223**, 569 (1989).
[50]C. L. Allyn, T. Gustaffson, and E. W. Plummer, Solid State Commun. **24**, 531 (1977).
[51]E. W. Jensen and T. F. Rhodin, Phys. Rev. B **27**, 3338 (1983).
[52]R. Miranda, K. Wandelt, D. Rieger, and R. D. Schnell, Surf. Sci. **139**, 430 (1984).
[53]P. Parneix, M. Büchner, G. Raseev, and N. Halberstadt, Chem. Phys. Lett. **233**, 430 (1995).
[54]P. Budau and G. Stan, Surf. Sci. (to be published).
[55]V. Fritzsche, K.-M. Schindler, P. Gardner, A. M. Bradshaw, M. C. Asensis, and D. P. Woodruff, Surf. Sci. **269/270**, 35 (1992).
[56]H. Le Rouzo and G. Raseev (unpublished).